Biomaterials and Biosystems 16 (2024) 100102

Contents lists available at ScienceDirect

Biomaterials and Biosystems

journal homepage: www.elsevier.com/locate/bbiosy

In vitro and in vivo assessment of a non-animal sourced chitosan scaffold loaded with xeno-free umbilical cord mesenchymal stromal cells cultured under macromolecular crowding conditions

Alessia Di Nubila [a], Meletios-Nikolaos Doulgkeroglou [a], Mehmet Gurdal [b], Stefanie H. Korntner [a], Dimitrios I. Zeugolis [a,b,*]

[a] Regenerative, Modular & Developmental Engineering Laboratory (REMODEL) and Science Foundation Ireland (SFI) Centre for Research in Medical Devices (CÚRAM), Biomedical Sciences Building, University of Galway, Galway, Ireland
[b] Regenerative, Modular & Developmental Engineering Laboratory (REMODEL), Charles Institute of Dermatology, Conway Institute of Biomolecular & Biomedical Research and School of Mechanical & Materials Engineering, University College Dublin (UCD), Dublin, Ireland

ARTICLE INFO

Keywords:
Xeno-free human umbilical cord mesenchymal stromal cells
Not-animal sourced chitosan scaffold
Macromolecular crowding
Advanced therapy medicinal products

ABSTRACT

There is an increasing demand to not only accelerate the development of advanced therapy tissue engineered medicines, but to also eliminate xenogeneic materials from their development cycle. With these in mind, herein we first assessed the influence of carrageenan as macromolecular crowding agent to enhance and accelerate extracellular matrix deposition in xeno-free human umbilical cord mesenchymal stromal cell cultures and we developed and characterised a non-animal sourced chitosan scaffold. Following appropriate in vitro experimentation, a splinted nude mouse wound healing model was used to assess wound closure and scar size of non-treated control, non-animal sourced chitosan scaffold, non-animal sourced chitosan scaffold loaded with xeno-free human umbilical cord mesenchymal stromal cells and non-animal sourced chitosan scaffold loaded with xeno-free human umbilical cord mesenchymal stromal cells cultured under macromolecular crowding conditions groups. Across all three donors, carrageenan supplementation significantly increased collagen deposition at day 5, day 8 and day 11 without affecting cell morphology, viability, DNA concentration and metabolic activity. Through freeze drying, a non-animal sourced chitosan sponge was developed with appropriate structural and mechanical properties for wound healing applications. In vitro biological analysis made apparent that neither the scaffold nor macromolecular crowding negatively impacted xeno-free human umbilical cord mesenchymal stromal cell metabolic activity and proliferation. In vivo biological analysis revealed no significant differences between the groups in wound closure and scar size, raising question about the suitability of the model. In any case, this work sets the foundations for the development of completely xeno-free tissue engineered medicines.

1. Introduction

Mesenchymal stromal cells (MSCs) are multipotent cells, capable of self-renewal and multi-lineage differentiation [1,2]. MSCs can be isolated from adult (e.g. bone marrow, fat) and foetal (umbilical cord, amnion) tissues [3,4]. Independently of the tissue origin, MSCs possess immunomodulatory properties and contribute to tissue homeostasis and regeneration, which make them valuable candidates for therapeutic applications [5,6]. However, adult MSCs require an invasive procedure to obtain them, thus compromising local tissue integrity and their quality, quantity, differentiation capacity and therapeutic potential are donor dependent, thus jeopardising patient therapeutic outcomes [7,8]. These limitations of the adult MSCs triggered investigations into the potential of foetal MSCs in regenerative medicine, with numerous reports now advocating their use [9,10] and pointing out their distinct advantages. For example, Wharton's jelly (a primordial mucous connective tissue of the human umbilical cord) contains primitive MSCs and yields the highest concentration of MSCs compared to other allogenic tissues [11]. Human umbilical cord mesenchymal stem cells (hUC-MSCs) are easily accessible and harvested with no risk to the donor. Further, hUC-MSCs offer several advantages over those sourced from adult tissues (e.g. higher proliferation rate, expansion capability

* Corresponding author at: REMODEL, UCD, Ireland.
E-mail address: dimitrios.zevgolis@ucd.ie (D.I. Zeugolis).

https://doi.org/10.1016/j.bbiosy.2024.100102
Received 26 March 2024; Received in revised form 6 June 2024; Accepted 8 October 2024
Available online 10 October 2024

and immunomodulatory properties) [12].

Clinical applications of any tissue engineered medicine may also be hampered by xenogeneic contaminations and inter-species disease transfer, caused by animal-derived cell culture media components and/or scaffolds. To this end, research and technology endeavours have been directed towards the development of xeno-free (XF) media formulation for cell culture purposes [13-16] and human recombinant biomolecules for implantable device purposes [17-20]. It is worth noting that XF media and human recombinant biomolecules have shown promising results with foetal [21-23] and adult [24-26], respectively, MSCs (albeit, the potential of human recombinant biomolecules with foetal MSCs has yet to be assessed).

A particular obstacle in the development of tissue engineered medicines is the prolonged in vitro expansion and/or culture times necessary to obtain the high cell numbers required for therapeutic effects and to develop an implantable device, respectively, that are associated with loss of phenotype and function [27-30]. It has been argued that extracellular matrix (ECM) facilitates maintenance of cell phenotype and function during in vitro culture [31], even under serum-free conditions [32]. Considering that in standard, deprived of macromolecules, culture conditions, the rate of ECM deposition is very slow, macromolecular crowding (MMC) has been introduced as a means to enhance and accelerate ECM deposition [33-35]. Among the different macromolecular crowders that have been tested, the sulphated polysaccharide carrageenan has been proved to induce the highest ECM deposition (up to 120-fold increase) in the shortest period of time (within 2–6 days in culture), due to its high polydispersity and negative charge [36,37]. It should be noted that although MMC has been extensively studied in non-human animal sera adult human MSC cultures [38-49], there are only two reports with MMC in XF adult human MSC cultures [50,51] and only one report in non-human animal sera foetal human MSC cultures [52]. Further, in preclinical setting, MMC has shown positive results in a scaffold-free conformation using adult human MSCs in non-human animal sera [46]. To-date, not only MMC has not been investigated in XF cultures of foetal human MSCs, but also no tissue engineered construct based on a XF scaffold, XF cultured foetal human MSCs and MMC has been assessed in preclinical setting.

With these in mind, herein we developed a XF tissue engineered medicine using MMC, XF hUC-MSCs and a non-animal sourced chitosan sponge and assessed its therapeutic potential in a mouse excisional wound splinting model (**Supplementary Schematic S1** provides the experimental design). This work essentially creates a blueprint for the development of a XF tissue engineered medicine.

2. Materials and methods

2.1. Materials

All chemicals, reagents, and tissue culture consumables were purchased from Sigma Aldrich (Ireland), unless otherwise stated. Carrageenan (Viscarin® GP 209 NF) was provided by FMC International Health and Nutrition (Ireland). XF hUC-MSCs (three donors) and appropriate media (RoosterBasal™-MSC) and supplements (RoosterBooster™-MSC-XF) were bought from RoosterBio® (USA). Chitosan powder (KiOsmetine®-CsH) was supplied by KitoZyme (Belgium).

2.2. Cell culture

The XF hUC-MSCs were cultured in RoosterNourish™-MSC-XF, using CellBIND®, Corning® plates. Cells were detached with TrypLE™ Select (Life Technologies, USA), an animal origin-free recombinant enzyme alternative to porcine or bovine trypsin. For cryopreservation, CryoStor® CS5 (STEMCELL Technologies, UK), a serum-free and animal component-free freezing media, was used. Cells at passage 4 were seeded at density of 25,000 cells/cm^2 and allowed to attach for 24 h at 37 °C in a humidified atmosphere of 5 % CO_2. After 24 h, the medium was replaced with medium containing various concentrations (10, 25, 50, 75 or 100 μg/ml) of carrageenan (CR) and 100 μM l-ascorbic acid 2-phosphate sesquimagnesium salt hydrate. Medium with 100 μM l-ascorbic acid 2-phosphate sesquimagnesium salt hydrate served as a control (-MMC). The cells were cultured for 5, 8 and 11 days.

2.3. Phase contrast microscopy analysis

XF hUC-MSCs morphology as function of donor, MMC and time in culture was assessed using an inverted brightfield microscope (Leica Microsystem, Germany). The experiment was conducted in three technical replicates per donor.

2.4. Cell viability analysis

Cell viability was assessed using the Live/Dead™ (ThermoFisher Scientific, UK) assay, as per manufacturer's procedure. Briefly, at each time point, cells were washed with Hank's Balanced Salt Solution (HBSS) and a solution of calcein AM at 4 μM and ethidium homodimer I at 2 μM was added. After 30 min incubation at 37 °C in a humidified atmosphere of 5 % CO_2, fluorescence images were acquired with an Olympus IX-81 inverted fluorescence microscope (Olympus Corporation, Japan). Cells treated with dimethyl sulfoxide were used as negative control. The experiment was conducted in three technical replicates per donor.

2.5. DNA concentration analysis

DNA concentration was quantified using the Quant-iT™ PicoGreen® dsDNA (ThermoFisher Scientific, UK) assay, as per manufacturer's protocol. Briefly, 250 μl of nucleic acid-free water was added to each well, the well plate was frozen at −80 °C and three freeze-thaw cycles were performed to lyse the cells and extract the DNA. 100 μl of each DNA sample were transferred into a 96-well plate. A standard curve was generated with 0, 200, 375, 500, 1000 and 2000 ng/ml DNA concentrations. 100 μl of PicoGreen® reagent at 1:200 dilution in 1X Tris-EDTA buffer was added to all standards and samples. Fluorescence values (excitation: 480 nm, emission: 520 nm) were detected with a Varioskan Flash Spectral scanning multimode reader (ThermoFisher Scientific, UK). DNA concentration was calculated using the standard curve. The experiment was conducted in three technical replicates per donor.

2.6. Cell metabolic activity analysis

Metabolic activity was evaluated using the alamarBlue® (Invitrogen, UK) assay, following the supplier's method. Briefly, samples were washed with HBSS and left in HBSS containing 10 % alamarBlue® for 3 h at 37 °C in a humidified atmosphere of 5 % CO_2. 100 μl of the alamarBlue® solution were transferred into a 96-well plate. Absorbance values were measured at 550 nm excitation and 595 nm emission with a Varioskan Flash Spectral scanning multimode reader (ThermoFisher Scientific, UK). Metabolic activity was expressed in terms of % of reduced alamarBlue™ dye normalised to the DNA quantity (ng/ml) obtained from the Quant-iT™ PicoGreen® dsDNA assay. Values were normalised to the -MMC control group. The experiment was conducted in three technical replicates per donor.

2.7. Electrophoresis analysis

Collagen deposition was quantified using sodium dodecyl sulphate-polyacrylamide gel electrophoresis (SDS-PAGE), based on established protocol of the group [53]. Briefly, at each time point media were aspired and cell layers were washed with HBSS. Subsequently, cell layers were digested with porcine gastric mucosa pepsin at a final concentration of 0.1 mg/ml in 0.05 M acetic acid (ThermoFisher Scientific, Ireland) and incubated for 2 h at 37 °C with gentle shaking. After

digestion, cell layers were scraped and neutralised with 0.1 N sodium hydroxide. 8 µl of cell layer solution were mixed with 34 µl of deionised water and 18 µl of sample buffer [0.25 g SDS (Bio-Rad Laboratories, UK) in 0.625 ml 1.25 M Tris–HCl (pH 6.8), 2 ml ultrapure water, glycerol (Bio-Rad Laboratories, UK) up to total volume of 5 ml and 1.25 mg bromophenol blue (Bio-Rad Laboratories, UK)]. The solution was briefly vortexed and denatured for 5 min at 95 °C. 10 µl of this solution were loaded per gel (3 % stacking gel and 5 % separation gel) lane and analysed (50 V for 30–40 min and 120 V 50–60 min) under non-reducing conditions with a Mini-Protean® 3 electrophoresis system (Bio-Rad Laboratories, UK). Bovine collagen type I (125 µg/ml, Symatese Biomateriaux, France) was used as control. Protein bands were stained with the SilverQuest™ kit (Invitrogen, UK) according to the manufacturer's protocol. The gels were imaged with a HP PrecisionScan Pro scanner (HP, UK). Densitometric analysis of the α1 and α2 bands was performed with ImageJ software (NIH, USA). The experiment was conducted in three technical replicates per donor.

2.8. Scaffold fabrication

A solution of 2 % (w/v) XF chitosan was prepared in acetic acid (1 % v/v in ultrapure water) and left overnight at room temperature under magnetic stirring. Then, the solution was poured into aluminium trays and frozen at −20 °C overnight. Frozen samples were lyophilised for 3 days (VirTis Advantage 2.0 Benchtop Freezer Dryer, Scientific Products, USA). Using a biopsy punch, round-shaped sponges were cut with a diameter of ~ 8.0 mm, thickness of ~ 2.1 mm and volume of ~ 105 mm^3. Sponges with this size were used for all in vitro experiments except for mechanical testing, which required specific dimensions to fit the tensile grips of the machine. For in vivo experiments, a smaller scaffold size (diameter of ~ 5.0 mm, thickness of ~ 2.1 mm and volume of ~ 41 mm^3) was used to match wound site dimensions.

2.9. Scaffold ultrastructural analysis

To assess pore size and distribution within the scaffolds, XF chitosan sponges were imaged with a Hitachi S-4700 scanning electron microscope (SEM, Hitachi High- Technologies Europe GmbH, Germany). Prior to imagining, samples were sectioned in the dry state, mounted onto a carbon disk and gold splutter coated (Emitech K-550X Sputter Coater, Emitech, UK). Experiments were performed in triplicates. From collected images, pore area was analysed using the ImageJ software (NIH, USA) with $N = 100$ for each sample. Porosity measurements were obtained by determining scaffold density (mass per unit volume). To assess sample volume, Archimedes' Principle was employed [54]. The following equation was used:

$$Porosity\ (\%) = \frac{w_w - w_0}{\rho\ V} * 100$$

(w_0: scaffold dry weight, w_w: scaffold weight after immersion in 100 % ethanol solution, ρ: ethanol density (0.79 mg/mm^3), V: scaffold volume).

2.10. Scaffold mechanical analysis

Mechanical properties (i.e. Young's modulus, yield stress, tensile strength, elongation at break) were analysed in tensile mode at an extension rate of 200 mm/min using a Universal testing machine (Zwick/Roell Z005, Germany), equipped with a load cell of 10 N. XF chitosan sponges with dimensions of 70.0 mm length, 10.0 mm width and 2.1 mm height were used. Experiments were performed in triplicate with samples in wet state (overnight incubation in HBSS). A tensile stress-strain curve was generated, and Young's modulus was calculated by drawing a tangent to the initial linear portion of the curve.

2.11. Scaffold swelling and in vitro degradation analyses

Swelling and in vitro degradation of the XF chitosan scaffolds were analysed by a gravimetric method. Experiments were performed in triplicates. First, sponges were immersed in a HBSS solution containing lysozyme from chicken egg white (10^4 U/ml), which shows a high enzymatic specificity to hydrolyse glycosidic bonds of chitosan [55,56], and kept at 37 °C. At each time point (1, 2, 5, 8, 11 and 22 days), HBSS was removed, and samples were weighed. Swelling ratio was estimated with the following calculation:

$$Swelling\ ratio\ (\%) = \frac{w_w - w_0}{w_0} * 100$$

(w_0: initial weight, w_w: wet sponge weight). Then, samples were kept at 37 °C for 24 h and weighed. Degradation was calculated using the following equation:

$$Degradation\ (\%) = \frac{w_0 - w_d}{w_0} * 100$$

(w_d: sponge dry weight). Results were presented as percentage degradation as a function of time.

2.12. Scaffold cell dose optimisation

Prior to XF hUC-MSC (donor 3) seeding, XF chitosan scaffolds were sterilised with a 70 % ethanol solution for 1 h, washed in HBSS, immersed in media and kept at 37 °C in a humidified atmosphere of 5 % CO_2 overnight. XF hUC-MSCs were then seeded at densities of 150, 300 and 600 k per sponge for 5, 8 and 11 days and cell distribution was assessed via nuclei staining. Experiments were performed in triplicates with cells from donor 3. Briefly, at each time point, sponges were washed with HBSS, fixed in 4 % paraformaldehyde, cryoprotected with 15 % and 30 % solutions of sucrose in HBSS (w/v), cryo-embedded and cryo-sectioned (10 µm thick sections) with a Leica Cryostat (Leica Biosystems, Germany). Sections were washed with HBSS and non-specific sites were blocked with 3 % bovine serum albumin for 30 min. Nuclei were stained with Hoechst 33,342 fluorescent stain (5 µl/ml in HBSS, ThermoFisher Scientific, UK) for 5 min and washed twice with HBSS. Images were then acquired using an Olympus IX-81 inverted fluorescence microscope (Olympus Corporation, Japan) and analysed with ImageJ software (NIH, USA). Nuclei were counted to assess cell number / area and therefore cell distribution throughout the scaffold. Based on results obtained, cell seeding density and required culture time prior to implantation were determined. DNA concentration and metabolic activity of optimal cell density were also quantified.

2.13. Mouse excisional wound splinting model

Animal studies were carried out under approval of the Animal Care Research Ethics Committee of the University of Galway (Approval number 15/DEC/07). A splinted nude mouse wound healing model was used [57-59]. In brief, 7–9 weeks old female athymic mice were anaesthetised with isoflurane, the skin of the dorsal area was disinfected with iodine and two full-thickness wounds of 5 mm in diameter were created using a punch biopsy. Silicone splints of 6 mm internal diameter and 12 mm external diameter were fixed around each wound with superglue and secured to the skin with 6–0 nylon sutures (Ethicon, Ireland) to prevent skin contraction. Prior to in vivo implantation, scaffolds were seeded with 600,000 hUC-MSCs (donor 3) and cultured for 8 days without (-MMC) and with CR (+MMC). Animals (five animals per group and two wounds per animal) were randomly assigned to a treatment group (both wounds) as follows: non-treated control (CTRL), XF chitosan scaffold (Scaffold), XF chitosan scaffold with XF hUC-MSCs and -MMC (Scaffold + Cells) and XF chitosan scaffold with XF hUC-MSCs and +MMC (Scaffold + Cells + MMC). After application of the treatment,

wounds were protected with Tegaderm™ (3 M, USA) dressing and adhesive bandages. At day 14, animals were euthanised by CO_2 overdose.

2.14. Wound closure rate and histological analyses

Wound closure rate and scar size were assessed as per previous publications [46,59]. Briefly, wound closure rate was determined by taking digital pictures of the wounds with a Redmi Note 8 Pro smartphone camera (Xiaomi, China) immediately post-surgery and at days 3, 7, 10 and 14. The planimetric area of the open wounds was measured using ImageJ (NIH, USA). Values were calculated as percentages of wound closure as follows:

$$Wound\ closure\ (\%) = \frac{(area\ of\ original\ wound\ --\ area\ of\ actual\ wound)}{area\ of\ original\ wound} * 100$$

For scar size assessment, tissue samples were harvested with an 8 mm biopsy punch and fixed in 4 % paraformaldehyde for 24 h at 4 °C. After processing of the tissue in a tissue processor (Excelsior AS, ThermoFisher Scientific, Ireland), samples were paraffin embedded and placed on a cold plate to solidify. Cross-sections of 5 μm in thickness were prepared from paraffin blocks by Microtechnical Services (Exeter, UK). The sections were deparaffinised in xylene and hydrated in descending concentrations of ethanol. Slides were stained using standard protocols for haematoxylin-eosin and Masson-Goldner's trichrome stainings in a Giotto automatic stainer (Diapath, Italy). The sections were then dehydrated in ascending solutions of ethanol and xylene and mounted using the Cristallo® liquid coverslipping technology (Diapath, Italy). Images were acquired using an Olympus BX51 optical microscope (Olympus Corporation, Japan) and analysed with ImageJ (NIH, USA). Scar size was calculated as follows:

$$Scar\ size\ (\mu m) = \frac{scar\ area\ (\mu m^2)}{avarage\ dermal\ thickness\ (\mu m)}$$

The thickness of neoformed epidermis was evaluated from haematoxylin-eosin stained images using the ImageJ line tool (NIH, USA), as per established in the literature protocol [59-62]. Seventy-five measurements (fifteen images, five measurements per image) of epidermal thickness per group were analysed. Collagen area was calculated by measuring with ImageJ (NIH, USA) the area in blue of Masson-Goldner's trichrome stained images [63,64]. Fifteen images per group were thresholded to isolate the blue stained collagen area and % area fraction of thresholded collagen-stained images was calculated. Granulocytes were manually counted from haematoxylin-eosin-stained images and averaged per unit area. Three 100×100 μm in size regions of interest from fifteen haematoxylin-eosin-stained images per group were analysed [65-67].

2.15. Statistical analysis

Data were processed using MINITAB® version 17 (Minitab Inc., USA) and reported as mean ± standard deviation. One-way analysis of variance (ANOVA) was used for multiple comparisons and Tukey's post hoc test was used for pairwise comparisons when the group distributions were normal (Anderson-Darling normality test) and the variances of populations were equal (Bonett's test and Levene's test). When either or both assumptions were violated, non-parametric analysis was conducted using Kruskal-Wallis test for multiple comparisons and Mann-Whitney test for pairwise comparisons. Results were considered statistically significant for $p < 0.05$.

3. Results

3.1. Basic hUC-MSC function analysis without and with MMC

Qualitative phase contrast microscopy analysis revealed no differences in cell morphology between the -MMC and the +MMC (independently of the CR concentration) groups at any time point and cell detachment was observed at day 8 and day 11 for the 50, 75 and 100 μg/ml CR concentrations (**Supplementary Figure S1**). Qualitative viability analysis revealed no differences in cell viability between the -MMC and the +MMC (independently of the CR concentration) groups at any time point and although cell detachment was observed at day 8 and day 11 for the 50, 75 and 100 μg/ml CR concentrations, the still attached cells were alive (**Supplementary Figure S2**). In general, DNA quantification analysis revealed no significant ($p > 0.05$) differences in DNA concentration between the -MMC and the +MMC (independently of the CR concentration) groups at a given time point (**Supplementary Figure S3**). In general, no significant ($p > 0.05$) differences were observed in metabolic activity between the -MMC and the +MMC (independently of the CR concentration) groups at a given time point (**Supplementary Figure S4**).

3.2. Electrophoresis analysis as a function of MMC

SDS-PAGE and complementary densitometric analysis for collagen α1(I) and α2(I) bands revealed that all CR concentrations (no significant, $p > 0.05$, difference between CR concentrations) significantly ($p < 0.05$) increased collagen type I deposition, in comparison to the -MMC group at a given time point (Fig. 1). All subsequent experiments were conducted with the 10 μg/ml CR concentration (lowest assessed effective concentration).

3.3. Scaffold characterisation

As evidenced by SEM analysis, the scaffolds were porous (Fig. 2A) with 0.022 ± 0.008 mm^2 and 89.9 ± 2.8 % pore area and porosity, respectively (Fig. 2B). Biomechanical analysis revealed that the scaffold had 946.0 ± 189.3 Pa, 15.4 ± 5.2 kPa, 31.7 ± 7.2 kPa and 38.8 ± 4.1 % Young's modulus, yield stress, tensile strength and elongation at break, respectively (Fig. 2B). Swelling analysis did not reveal any significant ($p > 0.05$) differences as a function of time (Fig. 2C). With respect to degradation, in comparison to day 1, there was an increase, albeit not significant ($p > 0.05$), at day 2 and day 5 and there was a significant ($p < 0.05$) increase at day 8, day 11 and day 22, but not significant, $p > 0.05$, between them (Fig. 2D).

3.4. Scaffold cell dose optimisation

Nuclei staining revealed that at day 5 and day 8, the 600 k cell density without and with CR allowed for the highest ($p < 0.05$) cell distribution within the chitosan scaffold, whilst at day 11, the 150 k cell density without and with CR showed the lowest ($p < 0.05$) cell distribution within the XF chitosan scaffold, with no significant, $p > 0.05$, difference between the 300 k and 600 k cell densities, independently of the absence or presence of CR (**Supplementary Figure S5**). DNA concentration and metabolic activity analyses revealed no significant ($p > 0.05$) differences between the -MMC and the +MMC groups at a given time point (**Supplementary Figure S6**).

Considering that the highest ($p < 0.05$) collagen deposition was observed at day 8 (Fig. 1) and the 600 k cell density induced the highest ($p < 0.05$) cell distribution at day 8 (**Supplementary Figure S5**), we selected this time point and cell density for preclinical assessment.

3.5. Wound closure rate and histological analyses

No signs of infection or necrotic tissue were found in any of the

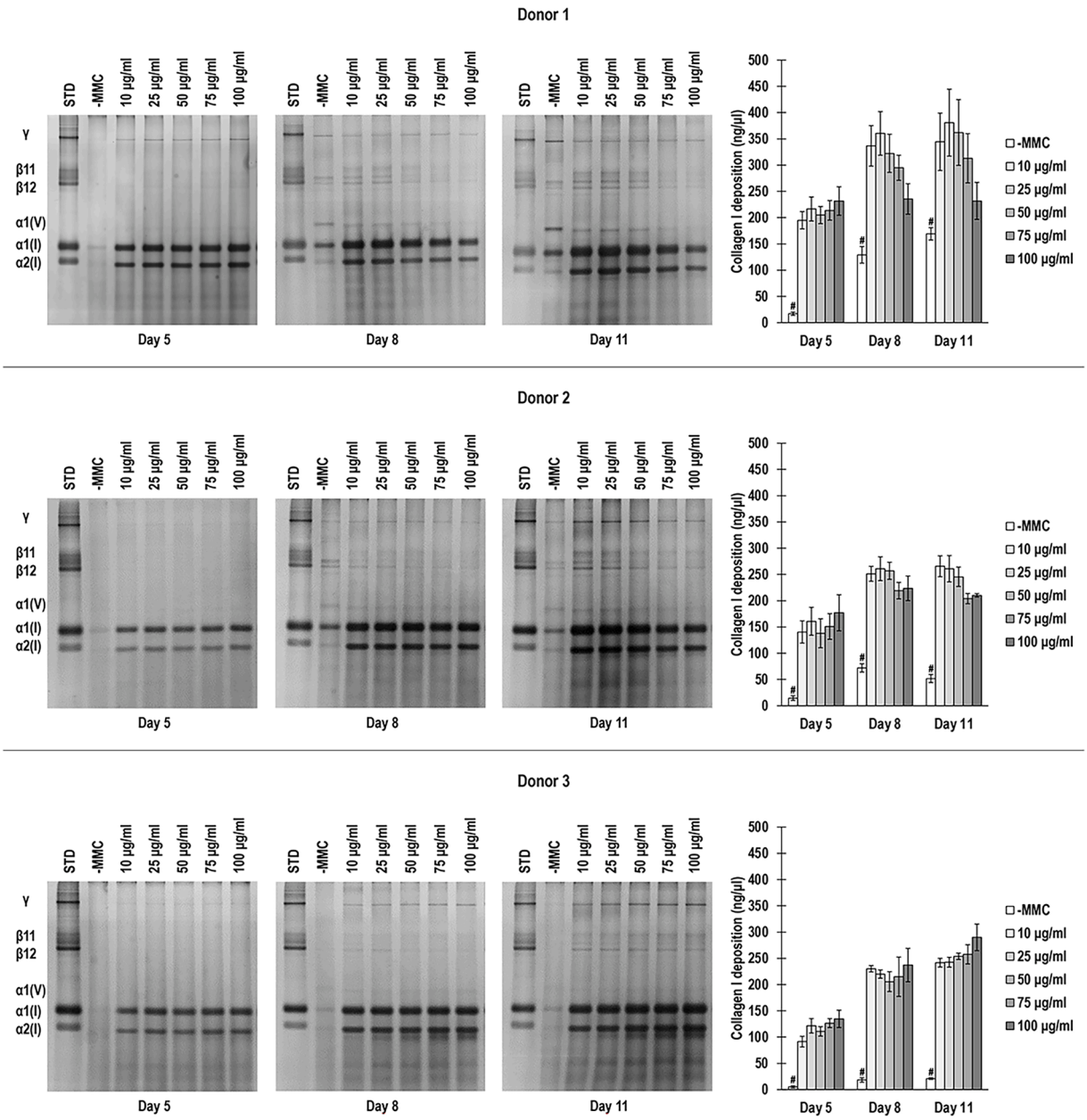

Fig. 1. SDS-PAGE and corresponding densitometric analysis of hUC-MSCs of donor 1, donor 2 and donor 3 at passage 4 after 5, 8 and 11 days of culture without and with increasing CR concentrations. Experiments were performed in 3 technical replicates per donor. # indicates the lowest ($p < 0.05$) population among all groups at a given time point.

groups at any time point. The splints were removed by the animals after day 3. All groups showed similar ($p > 0.05$) wound closure at a given time point (Fig. 3). At day 14, all groups showed similar ($p > 0.05$) scar size and epidermal thickness (Fig. 4) and collagen area fraction and granulocyte density (Fig. 5).

4. Discussion

Xenotransplantation (in the form of scaffold materials or culture media components), despite its well established history in biomedicine [68-71], harbours tremendous ethical, societal and safety concerns [72-76]. With this in mind, herein we developed and characterised a XF tissue engineered medicine using a XF chitosan scaffold and XF hUC-MSCs, cultured under MMC conditions.

4.1. MMC in XF hUC-MSC cultures

Although MMC has been used extensively in MSC cultures, only two reports have assessed its potential in XF cultures and both used adults MSC populations [50,51]. Considering that UC-MSCs are continuously gaining pace in tissue engineering and regenerative medicine [77-79], we first assessed the potential of MMC in XF hUC-MSC cultures. We selected CR as MMC agent, since its negative charge and high polydispersity index more effectively exclude available volume, thus resulting in the highest ECM deposition in the shortest period of time, in comparison to any other MMC agent assessed to-date [36,37]. Starting with basic cell function analysis, in general, CR did not affect cell morphology, DNA concentration, viability and proliferation, in agreement with numerous publications in the field in diverse range of cell populations (e.g. human dermal fibroblasts [36], human corneal fibroblasts [80], human tenocytes [81], human adipose derived MSCs [48],

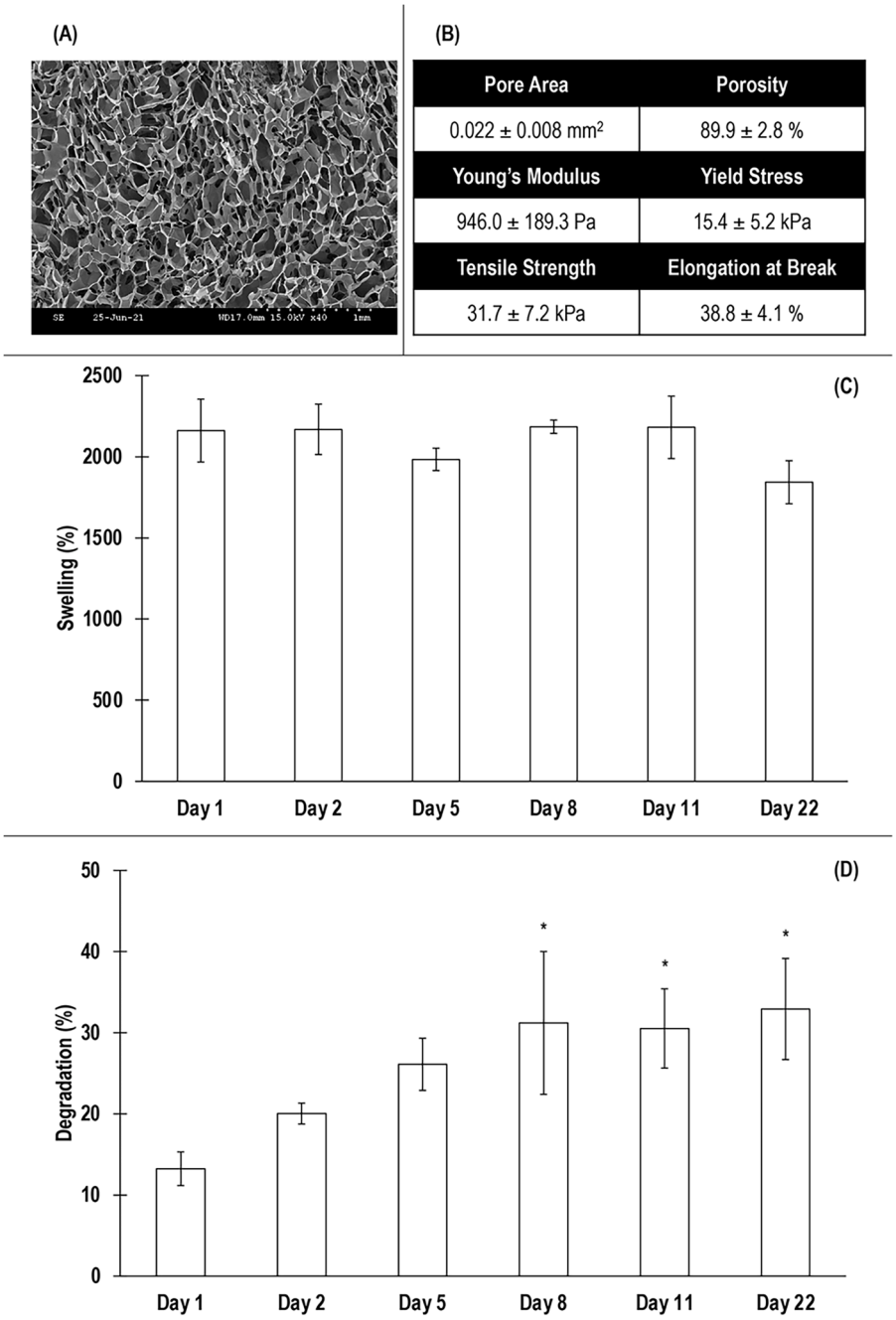

Fig. 2. Cross-sectional image of the non-animal sourced chitosan sponge (A). Physical and mechanical properties of the non-animal sourced chitosan sponge (B). Swelling (C) and degradation (D) of the non-animal sourced chitosan sponge over a 22 days period. Experiments were performed in 3 technical replicates. * indicates significant ($p < 0.05$) increase in comparison to day 1.

human bone marrow MSCs [43]). We recognise of course that at high CR concentrations cell detachment occurred, which has been observed before and was attributed to buoyancy of the cell-deposited ECM layer being stronger than the attachment forces between the culture plate and cell-deposited ECM layer [48]. With respect to ECM deposition, again our data align with previous publications where CR was shown to induced multi-fold increase in ECM deposition [36,80,81]. One should note that donor-dependent ECM deposition was observed, which is a well-established variable in MSC cultures [82-84], strongly suggesting that donor screening and selection is an essential step in the development of tissue engineered medicines.

4.2. XF chitosan scaffold characterisation and hUC-MSC loading without and with MMC

Chitosan, in many different conformations, is used extensively in biomedicine due to its good cytocompatibility and anti-bacterial, among others, properties [85-87]. Pore size, porosity and swelling capacity affect water retention, mechanical strength and cell adhesion and migration [88,89]. In our study, the lyophilized chitosan scaffolds exhibited suitable properties for hUC-MSC growth and wound healing applications, in accordance with previous reports in the field. For example, a chitosan scaffold with an average porosity of ~ 93 % and water uptake ratio of ~ 536 % sustained human dermal fibroblast attachment and infiltration [90]. In another study, human skin

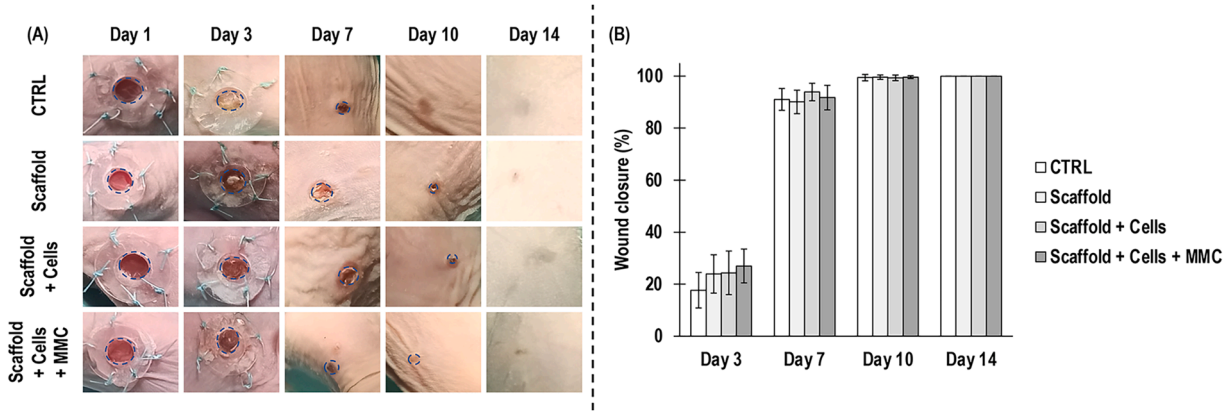

Fig. 3. Qualitative (A) and quantitative (B) wound closure analysis of non-treated control (CTRL), XF chitosan scaffold (Scaffold), XF chitosan scaffold with XF hUC-MSCs and -MMC (Scaffold + Cells) and XF chitosan scaffold with XF hUC-MSCs and +MMC (Scaffold + Cells + MMC) at day 3, day 7, day 10 and day 14. $N = 5$ animals per group.

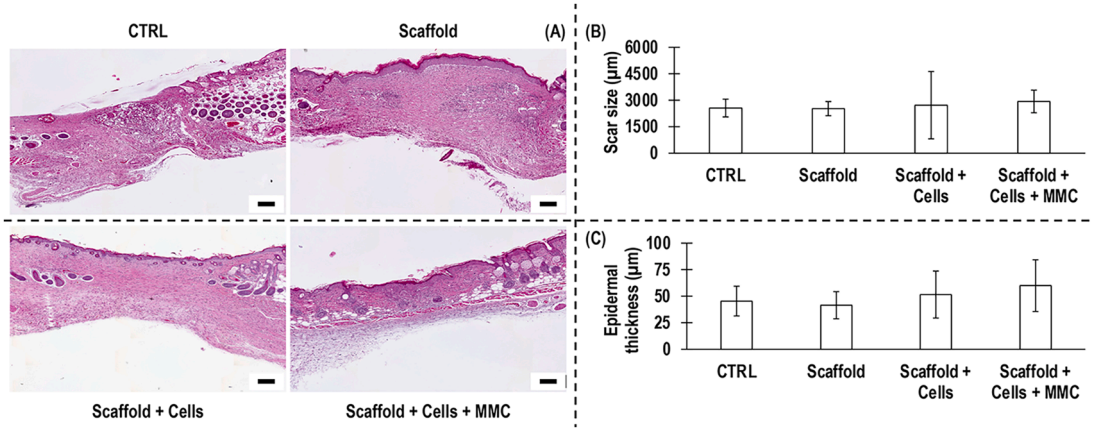

Fig. 4. Haematoxylin-eosin staining (A), scar size (B) and epidermal thickness (C) analyses of non-treated control (CTRL), XF chitosan scaffold (Scaffold), XF chitosan scaffold with XF hUC-MSCs and -MMC (Scaffold + Cells) and XF chitosan scaffold with XF hUC-MSCs and +MMC (Scaffold + Cells + MMC) at day 14. $N = 5$ animals per group. Scale bars: 250 µm.

fibroblasts were able to penetrate up to 400 µm into chitosan hydrogels fabricated using high pressure CO_2 with large pores (> 90 µm) and high porosities (> 85 %) [88]. The swelling ability of chitosan is inversely proportional to its degree of crystallinity [91,92], therefore a low degree of crystallinity in our chitosan scaffolds is responsible for a relatively low Young's modulus and tensile strength compared to mechanical properties of chitosan scaffolds with a high degree of crystallinity. For example, one study, targeting bone engineering applications, showed that scaffolds with chitosan concentrations ≥ 4 % exhibited a high degree of crystallinity and mechanical strength [93]. Our scaffolds, with a chitosan concentration of 2 %, were designed for skin wound healing applications that require an elastic and flexible scaffold [94]. The selected initial cell seeding density of 600 k hUC-MSCs, which has been used in both in vitro [95-97] and in vivo [59,98,99] studies for a broad range of cell populations, scaffolds and clinical indications, allowed for cell migration into the scaffold independently of the absence or presence of CR in culture. Proliferation and metabolic activity assays confirmed the scaffold's capacity to afford hUC-MSC growth, as has been shown before with various chitosan scaffold loaded with human osteoblasts [100], human dental pulp MSCs [101], immortalised human bone marrow MSCs [102] and human adipose-derived MSCs [103].

4.3. Preclinical analysis in a murine splinted wound healing model of XF chitosan scaffolds loaded with XF hUC-MSCs, cultured without and with MMC

At day 14, chitosan was not detected in skin wounds of scaffold groups by histological analysis, suggesting that either the scaffolds were degraded, despite in vitro data showing dry weight loss of only ~ 33 % at day 22 in comparison to day 0, or the animals had removed them. We feel that the former is the most likely scenario considering that previous studies have demonstrated a faster in vivo degradation rate of chitosan scaffolds when compared to in vitro degradation [104-106]. Further, in an in vivo rabbit critical size femur defect model, histological analysis revealed that chitosan scaffolds were present at day 7 and were completely degraded at day 30 [107]. In a subcutaneous rat model though, a collagen/chitosan scaffold was entirely absorbed by day 12 [108]. These results suggest that the rate of in vivo degradation / absorption of chitosan scaffolds depends on tissue and animal model. Epidermal thickness values were not significantly different among the different groups, although it has been shown for chitosan scaffolds to increase epidermis regeneration [109,110]. Regarding collagen content, although again no significant differences were observed between the groups, a chitosan scaffold loaded with human jaw bone marrow MSCs has been shown to induce an enhanced collagen deposition in rat calvarial defects [111]. Although one would have expected the presence of the scaffold to increase granulocyte density, no differences were

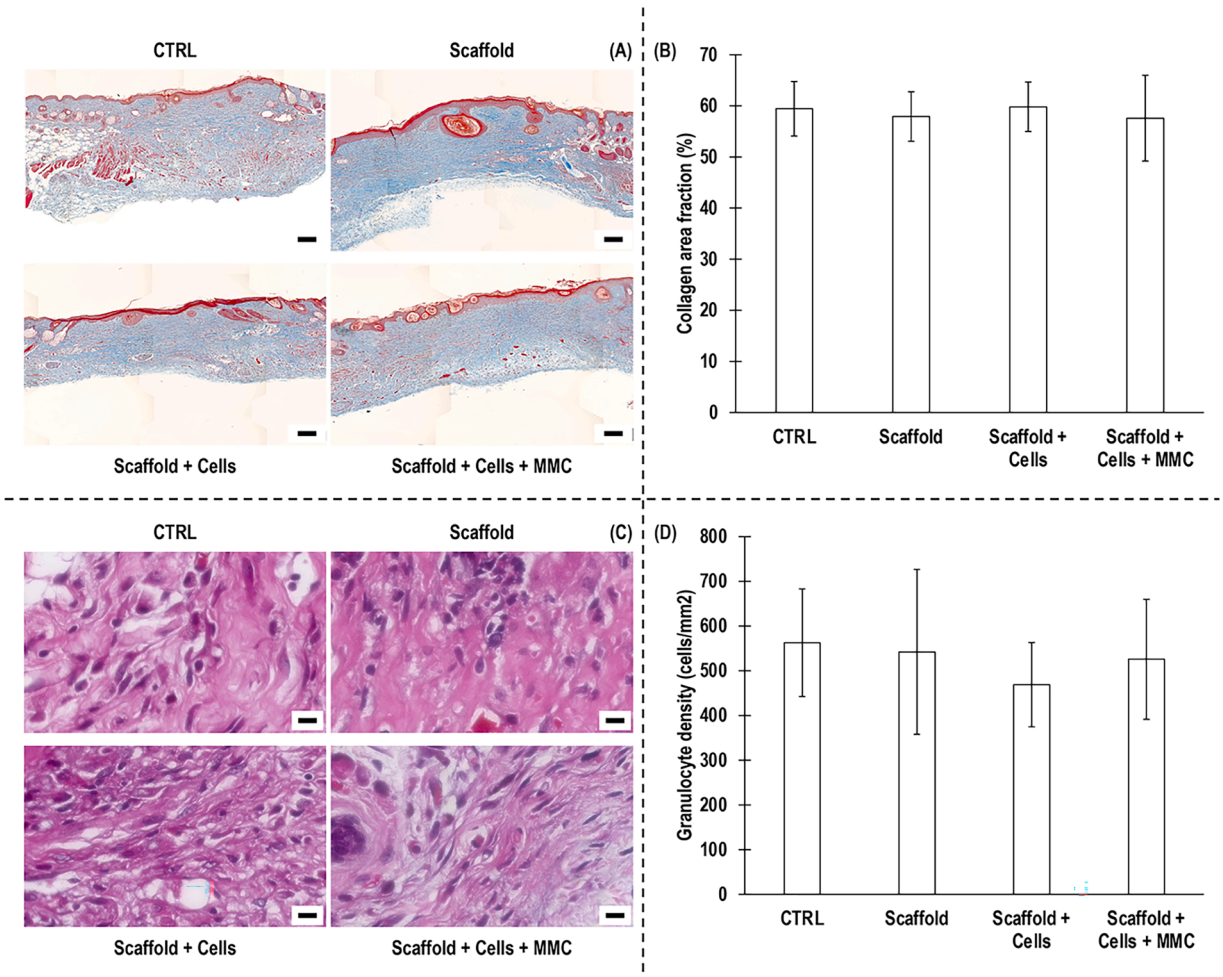

Fig. 5. Masson-Goldner's trichrome staining (A), collagen area fraction (B) haematoxylin-eosin staining (C) and granulocyte density (D) analyses of non-treated control (CTRL), XF chitosan scaffold (Scaffold), XF chitosan scaffold with XF hUC-MSCs and -MMC (Scaffold + Cells) and XF chitosan scaffold with XF hUC-MSCs and +MMC (Scaffold + Cells + MMC) at day 14. $N = 5$ animals per group. Scale bars for Masson-Goldner's trichrome images: 20 μm. Scale bars for haematoxylin-eosin images: 250 μm.

observed between the groups. Previous studies have reported that chitosan scaffolds have a chemotactic effect on immune cells [112] without eliciting a humoral immune response [113,114]. In general, chitosan scaffolds stimulate pro-inflammatory mediators, but anti-inflammatory effects can also be detected depending on the immune pathways that are activated [115,116]. These differences originate from the chitosan's degree of deacetylation, molecular weight and source [117,118]. One cannot exclude that the XF nature of the used herein chitosan scaffold may also have played a role in similar to the other groups granulocyte density.

With respect to wound closure, scar size, epidermal thickness, collagen area fraction and granulocyte density, no significant differences were observed between the groups. We know from the literature that MMC based therapies result in improved healing [46,119]. We also know that chitosan scaffolds promote wound healing [120,121], as do hUC-MSCs [122,123]. We feel that this indifference between the groups is due to the limitations of the model used that allowed the animals to remove the silicone rings and to bring about tissue contraction. Indeed, the silicone ring has been previously identified as major drawback of the model [124], with studies suggesting the use of Elizabethan collars and jackets with plastic wings [124] or wound chambers [125] or even shape memory alloys as internal splints [126] to avoid such issues. Unfortunately, none of these strategies were in our licence and therefore we were not able to use them. Investigators ought to publicise such limitations to inform future preclinical endeavours.

5. Conclusions

Here, we report for first time the development of a completely xeno-free tissue engineered medicine using xeno-free human umbilical cord mesenchymal stromal cells, macromolecular crowding and a non-animal sourced chitosan scaffold. Neither macromolecular crowding nor the non-animal sourced chitosan scaffold affected basic cell function. Macromolecular crowding significantly increased collagen deposition and the porous scaffolds allowed for cell infiltration. Preclinical assessment revealed no significant differences in wound closure and scar size between the groups (sham, scaffold, scaffold with cells and scaffold with cells and macromolecular crowding), largely attributed to the removal of splints (by the animals). Nonetheless, as neither infection nor necrotic tissues were observed, we consider the treatment as safe, albeit an appropriate animal model should be used to confirm efficiency and efficacy.

CRediT authorship contribution statement

Alessia Di Nubila: Writing – original draft, Methodology, Investigation, Formal analysis, Data curation. **Meletios-Nikolaos Doulgkeroglou:** Writing – review & editing, Methodology, Investigation, Formal analysis. **Mehmet Gurdal:** Writing – review & editing, Methodology, Investigation, Formal analysis. **Stefanie H. Korntner:** Writing – review & editing, Methodology, Investigation, Formal analysis. **Dimitrios I.**

Zeugolis: Writing – review & editing, Visualization, Supervision, Resources, Project administration, Funding acquisition, Conceptualization.

Declaration of competing interest

The authors declare that they have no known competing financial interests or personal relationships that could have appeared to influence the work reported in this paper.

Acknowledgements

This work has received funding from the European Research Council (ERC) under the European Union's Horizon 2020 research and innovation programme, grant agreement No 866126. This publication has emanated from research supported by Science Foundation Ireland (SFI) under grant number 19/FFP/6982. This work has received funding from the Irish Research Council, Government of Ireland, Postdoctoral Fellowship 2020, grant number GOIPD/2020/937. The authors would like to acknowledge the significant contribution of Dr Oonagh Dwane (University of Galway, Ireland) in the writing and management of all grants. The authors would like to thank Elena De Lucia (University of Galway, Ireland) and Giovanni Lauretta for technical support. The Graphical Abstract and the Supplementary Schematic S1 were prepared using bioRender.

Supplementary materials

Supplementary material associated with this article can be found, in the online version, at doi:10.1016/j.bbiosy.2024.100102.

Data availability

The raw data required to reproduce these findings are available on request from ADN and MND. The processed data required to reproduce these findings are available on request from ADN and MND.

References

[1] Pittenger MF, Discher DE, Peault BM, Phinney DG, Hare JM, Caplan AI. Mesenchymal stem cell perspective: cell biology to clinical progress. NPJ Regen Med 2019;4:22. https://doi.org/10.1038/s41536-019-0083-6.
[2] Ding DC, Shyu WC, Lin SZ. Mesenchymal stem cells. Cell Transplant 2011;20:5–14. https://doi.org/10.3727/096368910X.
[3] Zhao Q, Ren H, Han Z. Mesenchymal stem cells: immunomodulatory capability and clinical potential in immune diseases. J Cell Immunother 2016;2:3–20. https://doi.org/10.1016/j.jocit.2014.12.001.
[4] Song I, Rim J, Lee J, Jang I, Jung B, Kim K, Lee S. Therapeutic potential of human fetal mesenchymal stem cells in musculoskeletal disorders: a narrative review. Int J Mol Sci 2022;23:1439. https://doi.org/10.3390/ijms23031439.
[5] Maldonado V, Patel N, Smith E, Barnes C, Gustafson M, Rao R, Samsonraj R. Clinical utility of mesenchymal stem/stromal cells in regenerative medicine and cellular therapy. J Biol Eng 2023;17:44. https://doi.org/10.1186/s13036-023-00361-9.
[6] Huang Y, Wu Q, Tam P. Immunomodulatory mechanisms of mesenchymal stem cells and their potential clinical applications. Int J Mol Sci 2022;23:10023. https://doi.org/10.3390/ijms231710023.
[7] Mastrolia I, Foppiani E, Murgia A, Candini O, Samarelli A, Grisendi G, Veronesi E, Horwitz E, Dominici M. Challenges in clinical development of mesenchymal stromal/stem cells: concise review. Stem Cells Transl Med 2019;8:1135–48. https://doi.org/10.1002/sctm.19-0044.
[8] Zhou T, Yuan Z, Weng J, Pei D, Du X, He C, Lai P. Challenges and advances in clinical applications of mesenchymal stromal cells. J Hematol Oncol 2021;14:24. https://doi.org/10.1186/s13045-021-01037-x.
[9] Pu L, Meng M, Wu J, Zhang J, Hou Z, Gao H, Xu H, Liu B, Tang W, Jiang L, Li Y. Compared to the amniotic membrane, Wharton's jelly may be a more suitable source of mesenchymal stem cells for cardiovascular tissue engineering and clinical regeneration. Stem Cell Res Ther 2017;8:72. https://doi.org/10.1186/s13287-017-0501-x.
[10] Zhang H, Gu Y, Zhang K, Tu Y, Ouyang C. Roles and mechanisms of umbilical cord mesenchymal stem cells in the treatment of diabetic foot: a review of preclinical and clinical studies. J Diabetes Complications 2024;38:108671. https://doi.org/10.1016/j.jdiacomp.2023.108671.
[11] Gupta A, El-Amin 3rd SF, Levy HJ, Sze-Tu R, Ibim SE, Maffulli N. Umbilical cord-derived Wharton's jelly for regenerative medicine applications. J Orthop Surg Res 2020;15:49. https://doi.org/10.1186/s13018-020-1553-7.
[12] Badraiq H, Cvoro A, Galleu A, Simon M, Miere C, Hobbs C, Schulz R, Siow R, Dazzi F, Ilic D. Effects of maternal obesity on Wharton's Jelly mesenchymal stromal cells. Sci Rep 2017;7:17595. https://doi.org/10.1038/s41598-017-18034-1.
[13] van der Valk J, Brunner D, De Smet K, Fex Svenningsen A, Honegger P, Knudsen L, Lindl T, Noraberg J, Price A, Scarino M, Gstraunthaler G. Optimization of chemically defined cell culture media – Replacing fetal bovine serum in mammalian in vitro methods. Toxicol In Vitro 2010;24:1053–63. https://doi.org/10.1016/j.tiv.2010.03.016.
[14] Bui HTH, Nguyen LT, Than UTT. Influences of xeno-free media on mesenchymal stem cell expansion for clinical application. Tissue Eng Regen Med 2021;18:15–23. https://doi.org/10.1007/s13770-020-00306-z.
[15] Cimino M, Gonçalves R, Barrias C, Martins M. Xeno-free strategies for safe human mesenchymal stem/stromal cell expansion: supplements and coatings. Stem Cells Int 2017:6597815. https://doi.org/10.1155/2017/6597815. 2017.
[16] Bauman E, Granja P, Barrias C. Fetal bovine serum-free culture of endothelial progenitor cells-progress and challenges. J Tissue Eng Regen Med 2018;12:1567–78. https://doi.org/10.1002/term.2678.
[17] Paulini M, Camal Ruggieri I, Ramallo M, Alonso M, Rodriguez-Cabello J, Esbrit P, Mardegan Issa J, Feldman S. Recombinant proteins-based strategies in bone tissue engineering. Biomolecules 2021;12:3. https://doi.org/10.3390/biom12010003.
[18] Liu W, Lin H, Zhao P, Xing L, Li J, Wang Z, Ju S, Shi X, Liu Y, Deng G, Gao G, Sun L, Zhang X. A regulatory perspective on recombinant collagen-based medical devices. Bioact Mater 2021;12:198–202. https://doi.org/10.1016/j.bioactmat.2021.10.031.
[19] Chen Z, Fan D, Shang L. Exploring the potential of the recombinant human collagens for biomedical and clinical applications: a short review. Biomed Mater 2020;16:012001. https://doi.org/10.1088/1748-605X/aba6fa.
[20] Garcia Garcia C, Patkar S, Wang B, Abouomar R, Kiick K. Recombinant protein-based injectable materials for biomedical applications. Adv Drug Deliv Rev 2023;193:114673. https://doi.org/10.1016/j.addr.2022.114673.
[21] Swamynathan P, Venugopal P, Kannan S, Thej C, Kolkundar U, Bhagwat S, Ta M, Majumdar A, Balasubramanian S. Are serum-free and xeno-free culture conditions ideal for large scale clinical grade expansion of Wharton's jelly derived mesenchymal stem cells? A comparative study. Stem Cell Res Ther 2014;5:88. https://doi.org/10.1186/scrt477.
[22] Le H, Nguyen L, Hoang D, Bach T, Nguyen H, Mai H, Trinh D, Nguyen T, Nguyen L, Than U. Differential development of umbilical cord-derived mesenchymal stem cells during long-term maintenance in fetal bovine serum-supplemented medium and xeno- and serum-free culture. Cell Reprogram 2021;23:359–69. https://doi.org/10.1089/cell.2021.0050.
[23] Koh B, Sulaiman N, Fauzi M, Law J, Ng M, Yuan T, Azurah A, Mohd Yunus M, Idrus R, Yazid M. A three-dimensional xeno-free culture condition for Wharton's Jelly-mesenchymal stem cells: the pros and cons. Int J Mol Sci 2023;24:3745. https://doi.org/10.3390/ijms24043745.
[24] Muhonen V, Narcisi R, Nystedt J, Korhonen M, van Osch G, Kiviranta I. Recombinant human type II collagen hydrogel provides a xeno-free 3D microenvironment for chondrogenesis of human bone marrow-derived mesenchymal stromal cells. J Tissue Eng Regen Med 2017;11:843–54. https://doi.org/10.1002/term.1983.
[25] Parvizi M, Plantinga J, van Speuwel-Goossens C, van Dongen E, Kluijtmans S, Harmsen M. Development of recombinant collagen-peptide-based vehicles for delivery of adipose-derived stromal cells. J Biomed Mater Res A 2016;104:503–16. https://doi.org/10.1002/jbm.a.35588.
[26] Woo S, Choi J, Mo Y, Lee Y, Jeon W, Lee Y. Engineered elastin-like polypeptide improves the efficiency of adipose-derived stem cell-mediated cutaneous wound healing in type II diabetes mellitus. Heliyon 2023;9. https://doi.org/10.1016/j.heliyon.2023.e20201. e20201.
[27] Jeske R, Yuan X, Fu Q, Bunnell BA, Logan TM, Li Y. In vitro culture expansion shifts the immune phenotype of human adipose-derived mesenchymal stem cells. Front Immunol 2021;12:621744. https://doi.org/10.3389/fimmu.2021.621744.
[28] Yang YK, Ogando CR, Wang See C, Chang TY, Barabino GA. Changes in phenotype and differentiation potential of human mesenchymal stem cells aging in vitro. Stem Cell Res Ther 2018;9:131. https://doi.org/10.1186/s13287-018-0876-3.
[29] Zhang Y, Ravikumar M, Ling L, Nurcombe V, Cool SM. Age-related changes in the inflammatory status of human mesenchymal stem cells: implications for cell therapy. Stem Cell Reports 2021;16:694–707. https://doi.org/10.1016/j.stemcr.2021.01.021.
[30] Turinetto V, Vitale E, Giachino C. Senescence in human mesenchymal stem cells: functional changes and implications in stem cell-based therapy. Int J Mol Sci 2016;17:1164. https://doi.org/10.3390/ijms17071164.
[31] Pei M, He F, Kish VL. Expansion on extracellular matrix deposited by human bone marrow stromal cells facilitates stem cell proliferation and tissue-specific lineage potential. Tissue Eng Part A 2011;17:3067–76. https://doi.org/10.1089/ten.TEA.2011.0158.
[32] Rakian R, Block T, Johnson S, Marinkovic M, Wu J, Dai Q, Dean D, Chen X. Native extracellular matrix preserves mesenchymal stem cell "stemness" and differentiation potential under serum-free culture conditions. Stem Cell Res Ther 2015;6:235. https://doi.org/10.1186/s13287-015-0235-6.
[33] Zeugolis D. Bioinspired in vitro microenvironments to control cell fate: focus on macromolecular crowding. Am J Physiol Cell Physiol 2021;320:C842–9. https://doi.org/10.1152/ajpcell.00380.2020.

[34] Tsiapalis D, Zeugolis D. It is time to crowd your cell culture media – Physicochemical considerations with biological consequences. Biomaterials 2021; 275:120943. https://doi.org/10.1016/j.biomaterials.2021.120943.
[35] Raghunath M, Zeugolis DI. Transforming eukaryotic cell culture with macromolecular crowding. Trends Biochem Sci 2021;46:805–11. https://doi.org/10.1016/j.tibs.2021.04.006.
[36] Gaspar D, Fuller KP, Zeugolis DI. Polydispersity and negative charge are key modulators of extracellular matrix deposition under macromolecular crowding conditions. Acta Biomater 2019;88:197–210. https://doi.org/10.1016/j.actbio.2019.02.050.
[37] Satyam A, Kumar P, Fan X, Gorelov A, Rochev Y, Joshi L, Peinado H, Lyden D, Thomas B, Rodriguez B, Raghunath M, Pandit A, Zeugolis D. Macromolecular crowding meets tissue engineering by self-assembly: a paradigm shift in regenerative medicine. Advanced Materials 2014;26:3024–34. https://doi.org/10.1002/adma.201304428.
[38] Ang X, Lee M, Blocki A, Chen C, Ong L, Asada H, Sheppard A, Raghunath M. Macromolecular crowding amplifies adipogenesis of human bone marrow-derived mesenchymal stem cells by enhancing the pro-adipogenic microenvironment. Tissue Eng Part A 2014;20:966–81. https://doi.org/10.1089/ten.TEA.2013.0337.
[39] Gaspar D, Ryan C, Zeugolis D. Multifactorial bottom-up bioengineering approaches for the development of living tissue substitutes. FASEB J 2019;33: 5741–54. https://doi.org/10.1096/fj.201802451R.
[40] Graceffa V, Zeugolis D. Carrageenan enhances chondrogenesis and osteogenesis in human bone marrow stem cell culture. Eur Cell Mater 2019;37:310–32. https://doi.org/10.22203/eCM.v037a19.
[41] Guan S, Wu S, Li G, Xiao J, Gao B. Macromolecular crowding facilitates rapid fabrication of intact, robust cell sheets. Biotechnol Lett 2023;45:57–67. https://doi.org/10.1007/s10529-022-03336-w.
[42] Ryan CNM, Pugliese E, Shologu N, Gaspar D, Rooney P, Islam M, O'Riordan A, Biggs M, Griffin M, Zeugolis D. The synergistic effect of physicochemical in vitro microenvironment modulators in human bone marrow stem cell cultures. Biomater Adv 2023;144:213196. https://doi.org/10.1016/j.bioadv.2022.213196.
[43] Cigognini D, Gaspar D, Kumar P, Satyam A, Alagesan S, Sanz-Nogues C, Griffin M, O'Brien T, Pandit A, Zeugolis DI. Macromolecular crowding meets oxygen tension in human mesenchymal stem cell culture - A step closer to physiologically relevant in vitro organogenesis. Sci Rep 2016;6:30746. https://doi.org/10.1038/srep30746.
[44] Prewitz M, Stißel A, Friedrichs J, Träber N, Vogler S, Bornhäuser M, Werner C. Extracellular matrix deposition of bone marrow stroma enhanced by macromolecular crowding. Biomaterials 2015;73:60–9. https://doi.org/10.1016/j.biomaterials.2015.09.014.
[45] Lee MH, Goralczyk A, Kriszt R, Ang X, Badowski C, Li Y, Summers S, Toh S, Yassin M, Shabbir A, Sheppard A, Raghunath M. ECM microenvironment unlocks brown adipogenic potential of adult human bone marrow-derived MSCs. Sci Rep 2016;6:21173. https://doi.org/10.1038/srep21173.
[46] De Pieri A, Korntner S, Capella-Monsonis H, Tsiapalis D, Kostjuk S, Churbanov S, Timashev P, Gorelov A, Rochev Y, Zeugolis D. Macromolecular crowding transforms regenerative medicine by enabling the accelerated development of functional and truly three-dimensional cell assembled micro tissues. Biomaterials 2022;287:121674. https://doi.org/10.1016/j.biomaterials.2022.121674.
[47] Søndergaard RH, Højgaard L, Reese-Petersen A, Hoeeg C, Mathiasen A, Haack-Sørensen M, Follin B, Genovese F, Kastrup J, Juhl M, Ekblond A. Adipose-derived stromal cells increase the formation of collagens through paracrine and juxtacrine mechanisms in a fibroblast co-culture model utilizing macromolecular crowding. Stem Cell Res Ther 2022;13:250. https://doi.org/10.1186/s13287-022-02923-y.
[48] De Pieri A, Rana S, Korntner S, Zeugolis DI. Seaweed polysaccharides as macromolecular crowding agents. Int J Biol Macromol 2020;164:434–46. https://doi.org/10.1016/j.ijbiomac.2020.07.087.
[49] Zeiger AS, Loe F, Li R, Raghunath M, Van Vliet K. Macromolecular crowding directs extracellular matrix organization and mesenchymal stem cell behavior. PLoS One 2012;7:e37904. https://doi.org/10.1371/journal.pone.0037904.
[50] Korntner S, Di Nubila A, Gaspar D, Zeugolis D. Macromolecular crowding in animal component-free, xeno-free and foetal bovine serum media for human bone marrow mesenchymal stromal cell expansion and differentiation. Front Bioeng Biotechnol 2023;11:1136827. https://doi.org/10.3389/fbioe.2023.1136827.
[51] Patrikoski M, Lee M, Mäkinen L, Ang X, Mannerström B, Raghunath M, Miettinen S. Effects of macromolecular crowding on human adipose stem cell culture in fetal bovine serum, human serum, and defined xeno-free/serum-free conditions. Stem Cells Int 2017:6909163. https://doi.org/10.1155/2017/6909163. 2017.
[52] Du S, Elliman S, Zeugolis D, O'Brien T. Carrageenan as a macromolecular crowding agent in human umbilical cord derived mesenchymal stromal cell culture. Int J Biol Macromol 2023;251:126353. https://doi.org/10.1016/j.ijbiomac.2023.126353.
[53] Capella-Monsonis H, Coentro JQ, Graceffa V, Wu Z, Zeugolis DI. An experimental toolbox for characterization of mammalian collagen type I in biological specimens. Nat Protoc 2018;13:507–29. https://doi.org/10.1038/nprot.2017.117.
[54] Bertoldi S, Fare S, Tanzi MC. Assessment of scaffold porosity: the new route of micro-CT. J Appl Biomater Biomech 2011;9:165–75. https://doi.org/10.5301/JABB.2011.8863.
[55] Islam N, Dmour I, Taha MO. Degradability of chitosan micro/nanoparticles for pulmonary drug delivery. Heliyon 2019;5. https://doi.org/10.1016/j.heliyon.2019.e01684. e01684.
[56] Kim S, Fan J, Lee CS, Lee M. Dual functional lysozyme-chitosan conjugate for tunable degradation and antibacterial activity. ACS Appl Bio Mater 2020;3: 2334–43. https://doi.org/10.1021/acsabm.0c00087.
[57] Wang X, Ge J, Tredget EE, Wu Y. The mouse excisional wound splinting model, including applications for stem cell transplantation. Nat Protoc 2013;8:302–9. https://doi.org/10.1038/nprot.2013.002.
[58] Lam MT, Nauta A, Meyer NP, Wu JC, Longaker MT. Effective delivery of stem cells using an extracellular matrix patch results in increased cell survival and proliferation and reduced scarring in skin wound healing. Tissue Eng Part A 2013; 19:738–47. https://doi.org/10.1089/ten.TEA.2012.0480.
[59] Capella-Monsonis H, De Pieri A, Peixoto R, Korntner S, Zeugolis DI. Extracellular matrix-based biomaterials as adipose-derived stem cell delivery vehicles in wound healing: a comparative study between a collagen scaffold and two xenografts. Stem Cell Res Ther 2020;11:510. https://doi.org/10.1186/s13287-020-02021-x.
[60] Vazquez-Zapien GJ, Martinez-Cuazitl A, Granados-Jimenez A, Sanchez-Brito M, Guerrero-Ruiz M, Camacho-Ibarra A, Miranda-Ruiz MA, Dox-Aguillon IS, Ramirez-Torres JA, Mata-Miranda MM. Skin wound healing improvement in diabetic mice through FTIR microspectroscopy after implanting pluripotent stem cells. APL Bioeng 2023;7:016109. https://doi.org/10.1063/5.0130383.
[61] Shibuya Y, Hokugo A, Okawa H, Kondo T, Khalil D, Wang L, Roca Y, Clements A, Sasaki H, Berry E, Nishimura I, Jarrahy R. Therapeutic downregulation of neuronal PAS domain 2 (Npas2) promotes surgical skin wound healing. Elife 2022;11. https://doi.org/10.7554/eLife.71074. e71074.
[62] Guo Y, Dreier JR, Cao J, Du H, Granter SR, Kwiatkowski DJ. Analysis of a mouse skin model of tuberous sclerosis complex. PLoS One 2016;11. https://doi.org/10.1371/journal.pone.0167384. e0167384.
[63] Ying C, Qi Y, Cang-Bao X. A convenient method for quantifying collagen fibers in atherosclerotic lesions by ImageJ software. Int J Clin Exp Med 2017;10: 14904–10.
[64] Kuo CK, Tuan RS. Mechanoactive tenogenic differentiation of human mesenchymal stem cells. Tissue Eng Part A 2008;14:1615–27. https://doi.org/10.1089/ten.tea.2006.0415.
[65] Garcia-Mendoza MG, Inman DR, Ponik SM, Jeffery JJ, Sheerar DS, Van Doorn RR, Keely PJ. Neutrophils drive accelerated tumor progression in the collagen-dense mammary tumor microenvironment. Breast Cancer Res 2016;18:49. https://doi.org/10.1186/s13058-016-0703-7.
[66] Chan JK. The wonderful colors of the hematoxylin-eosin stain in diagnostic surgical pathology. Int J Surg Pathol 2014;22:12–32. https://doi.org/10.1177/1066896913517939.
[67] Wano N, Sanguanrungsirikul S, Keelawat S, Somboonwong J. The effects of whole-body vibration on wound healing in a mouse pressure ulcer model. Heliyon 2021;7. https://doi.org/10.1016/j.heliyon.2021.e06893. e06893.
[68] Yao Q, Zheng Y, Lan Q, Kou L, Xu H, Zhao Y. Recent development and biomedical applications of decellularized extracellular matrix biomaterials. Mater Sci Eng C Mater Biol Appl 2019;104:109942. https://doi.org/10.1016/j.msec.2019.109942.
[69] Capella-Monsonís H, Zeugolis D. Decellularized xenografts in regenerative medicine: from processing to clinical application. Xenotransplantation 2021;28. https://doi.org/10.1111/xen.12683. e12683.
[70] Zhe M, Wu X, Yu P, Xu J, Liu M, Yang G, Xiang Z, Xing F, Ritz U. Recent advances in decellularized extracellular matrix-based bioinks for 3D bioprinting in tissue engineering. Materials (Basel) 2023;16:3197. https://doi.org/10.3390/ma16083197.
[71] Cassotta M, Bartnicka J, Pistollato F, Parvatam S, Weber T, D'Alessandro V, Bastos L, Coecke S. A worldwide survey on the use of animal-derived materials and reagents in scientific experimentation. Eng Life Sci 2022;22:564–83. https://doi.org/10.1002/elsc.202100167.
[72] Boneva R, Folks T, Chapman L. Infectious disease issues in xenotransplantation. Clin Microbiol Rev 2001;14:1–14. https://doi.org/10.1128/CMR.14.1.1-14.2001.
[73] Rollin B. Ethical and societal issues occasioned by xenotransplantation. Animals (Basel) 2020;10:1695. https://doi.org/10.3390/ani10091695.
[74] Zhai X. Xenotransplantation — Reflections on the bioethics. Health Care Sci 2022;1:86–92. https://doi.org/10.1002/hcs2.18.
[75] Arabi T, Sabbah B, Lerman A, Zhu X, Lerman L. Xenotransplantation: current challenges and emerging solutions. Cell Transplant 2023;32:9636897221148771. https://doi.org/10.1177/09636897221148771.
[76] Tekkatte C, Gunasingh G, Cherian K, Sankaranarayanan K. "Humanized" stem cell culture techniques: the animal serum controversy. Stem Cells Int 2011:504723. https://doi.org/10.4061/2011/504723. 2011.
[77] Chetty S, Yarani R, Swaminathan G, Primavera R, Regmi S, Rai S, Zhong J, Ganguly A, Thakor A. Umbilical cord mesenchymal stromal cells-from bench to bedside. Front Cell Dev Biol 2022;10:1006295. https://doi.org/10.3389/fcell.2022.1006295.
[78] Zhang Y, Zhuang H, Ren X, Jiang F, Zhou P. Therapeutic effects of different intervention forms of human umbilical cord mesenchymal stem cells in the treatment of osteoarthritis. Front Cell Dev Biol 2023;11:1246504. https://doi.org/10.3389/fcell.2023.1246504.
[79] Can A, Celikkan F, Cinar O. Umbilical cord mesenchymal stromal cell transplantations: a systemic analysis of clinical trials. Cytotherapy 2017;19: 1351–82. https://doi.org/10.1016/j.jcyt.2017.08.004.
[80] Kumar P, Satyam A, Fan X, Rochev Y, Rodriguez B, Gorelov A, Joshi L, Raghunath M, Pandit A, Zeugolis D. Accelerated development of supramolecular corneal stromal-like assemblies from corneal fibroblasts in the presence of macromolecular crowders. Tissue Eng Part C Methods 2015;21:660–70.

[81] Tsiapalis D, De Pieri A, Spanoudes K, Sallent I, Kearns S, Kelly J, Raghunath M, Zeugolis D. The synergistic effect of low oxygen tension and macromolecular crowding in the development of extracellular matrix-rich tendon equivalents. Biofabrication 2020;12:025018. https://doi.org/10.1088/1758-5090/ab6412.
[82] Kang I, Lee B, Choi S, Lee J, Kim J, Kim B, Kim D, Lee S, Shin N, Seo Y, Kim H, Kim D, Kang K. Donor-dependent variation of human umbilical cord blood mesenchymal stem cells in response to hypoxic preconditioning and amelioration of limb ischemia. Exp Mol Med 2018;50:1–15. https://doi.org/10.1038/s12276-017-0014-9.
[83] Bogers S, Barrett J. Three-dimensional culture of equine bone marrow-derived mesenchymal stem cells enhances anti-inflammatory properties in a donor-dependent manner. Stem Cells Dev 2022;31:777–86. https://doi.org/10.1089/scd.2022.0074.
[84] Siennicka K, Zołocińska A, Dębski T, Pojda Z. Comparison of the donor age-dependent and in vitro culture-dependent mesenchymal stem cell aging in rat model. Stem Cells Int 2021;2021:6665358. https://doi.org/10.1155/2021/6665358.
[85] Ahmed S, Ikram S. Chitosan based scaffolds and their applications in wound healing. Achiev Life Sci 2016;10:27–37. https://doi.org/10.1016/j.als.2016.04.001.
[86] Che X, Zhao T, Hu J, Yang K, Ma N, Li A, Sun Q, Ding C, Ding Q. Application of chitosan-based hydrogel in promoting wound healing: a review. Polymers (Basel) 2024;16:344. https://doi.org/10.3390/polym16030344.
[87] Elizalde-Cárdenas A, Ribas-Aparicio R, Rodríguez-Martínez A, Leyva-Gómez G, Ríos-Castañeda C, González-Torres M. Advances in chitosan and chitosan derivatives for biomedical applications in tissue engineering: an updated review. Int J Biol Macromol 2024;262:129999. https://doi.org/10.1016/j.ijbiomac.2024.129999.
[88] Ji C, Khademhosseini A, Dehghani F. Enhancing cell penetration and proliferation in chitosan hydrogels for tissue engineering applications. Biomaterials 2011;32:9719–29. https://doi.org/10.1016/j.biomaterials.2011.09.003.
[89] Tao L, Zhonglong L, Ming X, Zezheng Y, Zhiyuan L, Xiaojun Z, Jinwu W. In vitro and in vivo studies of a gelatin/carboxymethyl chitosan/LAPONITE® composite scaffold for bone tissue engineering. RSC Adv 2017;7:54100–10. https://doi.org/10.1039/c7ra06913h.
[90] Hilmi A, Halim A, Hassan A, Lim C, Noorsal K, Zainol I. In vitro characterization of a chitosan skin regenerating template as a scaffold for cells cultivation. SpringerPlus 2013;2:79. https://doi.org/10.1186/2193-1801-2-79.
[91] Ioelovich MY. Crystallinity and hydrophility of chitin and chitosan. Res Rev J Chem 2014;3:7–14.
[92] Wan Y, Wu H, Cao X, Dalai S. Compressive mechanical properties and biodegradability of porous poly(caprolactone)/chitosan scaffolds. Polym Degrad Stab 2008;93:1736–41. https://doi.org/10.1016/j.polymdegradstab.2008.08.001.
[93] Jana S, Florczyk SJ, Leung M, Zhang M. High-strength pristine porous chitosan scaffolds for tissue engineering. J Mater Chem 2012;22:6291–9. https://doi.org/10.1039/c2jm16676c.
[94] Rodriguez-Cabello JC, Gonzalez de Torre I, Ibanez-Fonseca A, Alonso M. Bioactive scaffolds based on elastin-like materials for wound healing. Adv Drug Deliv Rev 2018;129:118–33. https://doi.org/10.1016/j.addr.2018.03.003.
[95] Skiles ML, Fancy R, Topiwala P, Sahai S, Blanchette J. Correlating hypoxia with insulin secretion using a fluorescent hypoxia detection system. J Biomed Mater Res B Appl Biomater 2011;97:148–55. https://doi.org/10.1002/jbm.b.31796.
[96] Grenier J, David B, Journé C, Cicha I, Letourneur D, Duval H. Perfusion of MC3T3E1 preosteoblast spheroids within polysaccharide-based hydrogel scaffolds: an experimental and numerical study at the bioreactor scale. Bioengineering (Basel) 2023;10:849. https://doi.org/10.3390/bioengineering10070849.
[97] Krug C, Beer A, Hartmann B, Prein C, Clause-Schaumann H, Holzbach T, Aszodi A, Giunta R, Saller M, Volkmer E. Fibrin glue displays promising in vitro characteristics as a potential carrier of adipose progenitor cells for tissue regeneration. J Tissue Eng Regen Med 2019;13:359–68. https://doi.org/10.1002/term.2778.
[98] Luo G, Cheng W, He W, Wang X, Tan J, Fitzgerald M, Li X, Wu J. Promotion of cutaneous wound healing by local application of mesenchymal stem cells derived from human umbilical cord blood. Wound Repair Regen 2010;18:506–13. https://doi.org/10.1111/j.1524-475X.2010.00616.x.
[99] Chatterjea A, LaPointe V, Alblas J, Chatterjea S, van Blitterswijk C, de Boer J. Suppression of the immune system as a critical step for bone formation from allogeneic osteoprogenitors implanted in rats. J Cell Mol Med 2014;18:134–42. https://doi.org/10.1111/jcmm.12172.
[100] Silvestro I, Sergi R, Scotto d'Abusco A, Mariano A, Martinelli A, Piozzi A, Francolini I. Chitosan scaffolds with enhanced mechanical strength and elastic response by combination of freeze gelation, photo-crosslinking and freeze-drying. Carbohydr Polym 2021;267:118156. https://doi.org/10.1016/j.carbpol.2021.118156.
[101] Leite YKdC, Oliveira ACdJ, Quelemes PV, Neto NMA, Carvalho CESd, Soares Rodrigues HW, Alves MMdM, Carvalho FAdA, Arcanjo DDR, Silva-Filho ECd, Durazzo A, Lucarini M, Carvalho MAMd, Silva DAd, Leite JRdSdA. Novel scaffold based on chitosan hydrogels/phthalated cashew gum for supporting human dental pulp stem cells. Pharmaceuticals 2023;16:266. https://doi.org/10.3390/ph16020266.
[102] Pitrolino KA, Felfel RM, Pellizzeri LM, McLaren J, Popov AA, Sottile V, Scotchford CA, Scammell BE, Roberts GAF, Grant DM. Development and in vitro assessment of a bi-layered chitosan-nano-hydroxyapatite osteochondral scaffold. Carbohydr Polym 2022;282:119126. https://doi.org/10.1016/j.carbpol.2022.119126.
[103] Wang J, Zhou L, Sun Q, Cai H, Tan WS. Porous chitosan derivative scaffolds affect proliferation and osteogenesis of mesenchymal stem cell via reducing intracellular ROS. Carbohydr Polym 2020;237:116108. https://doi.org/10.1016/j.carbpol.2020.116108.
[104] Wang J, Fu S, Li H, Wu Y. A CS-based composite scaffold with excellent photothermal effect and its application in full-thickness skin wound healing. Regen Biomater 2023;10. https://doi.org/10.1093/rb/rbad028. rbad028.
[105] Ren D, Yi H, Wang W, Ma X. The enzymatic degradation and swelling properties of chitosan matrices with different degrees of N-acetylation. Carbohydr Res 2005;340:2403–10. https://doi.org/10.1016/j.carres.2005.07.022.
[106] Abourehab MAS, Pramanik S, Abdelgawad MA, Abualsoud BM, Kadi A, Ansari MJ, Deepak A. Recent advances of chitosan formulations in biomedical applications. Int J Mol Sci 2022;23:1–45. https://doi.org/10.3390/ijms231810975.
[107] Qasim SB, Husain S, Huang Y, Pogorielov M, Deineka V, Lyndin M, Rawlinson A, Rehman IU. In- vitro and in -vivo degradation studies of freeze gelated porous chitosan composite scaffolds for tissue engineering applications. Polym Degrad Stab 2017;136:31–8. https://doi.org/10.1016/j.polymdegradstab.2016.11.018.
[108] Fu F, Zhu X, Qin Z, Wang JJ, Xu C, Wang LN, Tu Y, Zhang S, Li RX, Li XH, Zhao ML. Differential degradation rate and underlying mechanism of a collagen/chitosan complex in subcutis, spinal cord and brain tissues of rat. J Mater Sci Mater Med 2018;29:35. https://doi.org/10.1007/s10856-018-6033-9.
[109] Seyyed Tabaei SJ, Rahimi M, Akbaribazm M, Ziai SA, Sadri M, Shahrokhi SR, Rezaei MS. Chitosan-based nano-scaffolds as antileishmanial wound dressing in BALB/c mice treatment: characterization and design of tissue regeneration. Iran J Basic Med Sci 2020;23:788–99. https://doi.org/10.22038/ijbms.2020.41361.9770.
[110] El-Shaer AJ, Badr HA, AlSadek DM. The combined effect of the human umbilical cord blood with chitosan scaffold on the full-thickness wound healing process in rats. Iraqi J Vet Sci 2023;37:391–403. https://doi.org/10.33899/ijvs.2022.134782.2404.
[111] Zang S, Zhu2 L, Luo K, Mu R, Chen F, Wei X, Yan X, Han B, Shi X, Wang Q, Jin L. Chitosan composite scaffold combined with bone marrow-derived mesenchymal stem cells for bone regeneration: in vitro and in vivo evaluation. Oncotarget 2017;8:110890–903.
[112] Almeida CR, Serra T, Oliveira MI, Planell JA, Barbosa MA, Navarro M. Impact of 3-D printed PLA- and chitosan-based scaffolds on human monocyte/macrophage responses: unraveling the effect of 3-D structures on inflammation. Acta Biomater 2014;10:613–22. https://doi.org/10.1016/j.actbio.2013.10.035.
[113] VandeVord PJ, Matthew HW, DeSilva SP, Mayton L, Wu B, Wooley PH. Evaluation of the biocompatibility of a chitosan scaffold in mice. J Biomed Mater Res 2002;59:585–90. https://doi.org/10.1002/jbm.1270.
[114] Viveros-Moreno NG, Garcia-Lorenzana M, Pena-Mercado E, Garcia-Sanmartin J, Narro-Iniguez J, Salazar-Garcia M, Huerta-Yepez S, Sanchez-Gomez C, Martinez A, Beltran-Vargas NE. In vivo biocompatibility testing of nanoparticle-functionalized alginate-chitosan scaffolds for tissue engineering applications. Front Bioeng Biotechnol 2023;11:1295626. https://doi.org/10.3389/fbioe.2023.1295626.
[115] Lin W, Qi X, Guo W, Liang D, Chen H, Lin B, Deng X. A barrier against reactive oxygen species: chitosan/acellular dermal matrix scaffold enhances stem cell retention and improves cutaneous wound healing. Stem Cell Res Ther 2020;11:383. https://doi.org/10.1186/s13287-020-01901-6.
[116] Oliveira MI, Santos SG, Oliveira MJ, Torres AL, Barbosa MA. Chitosan drives anti-inflammatory macrophage polarisation and pro-inflammatory dendritic cell stimulation. Eur Cell Mater 2012;24:136–53. https://doi.org/10.22203/ecm.v024a10.
[117] Lima BV, Oliveira MJ, Barbosa MA, Gonçalves RM, Castro F. Harnessing chitosan and poly-(γ-glutamic acid)-based biomaterials towards cancer immunotherapy. Mater Today Adv 2022;15:100252. https://doi.org/10.1016/j.mtadv.2022.100252.
[118] Simard P, Galarneau H, Marois S, Rusu D, Hoemann CD, Poubelle PE, El-Gabalawy H, Fernandes MJ. Neutrophils exhibit distinct phenotypes toward chitosans with different degrees of deacetylation: implications for cartilage repair. Arthritis Res Ther 2009;11. https://doi.org/10.1186/ar2703. R74.
[119] Chiang C, Fang Y, Ho C, Assunção M, Lin S, Wang Y, Blocki A, Huang C. Bioactive decellularized extracellular matrix derived from 3D stem cell spheroids under macromolecular crowding serves as a scaffold for tissue engineering. Adv Healthc Mater 2021;10. https://doi.org/10.1002/adhm.202100024. e2100024.
[120] Vazquez-Ayala L, Del Ángel-Olarte C, Escobar-García D, Rosales-Mendoza S, Solis-Andrade I, Pozos-Guillén A, Palestino G. Chitosan sponges loaded with metformin and microalgae as dressing for wound healing: a study in diabetic bio-models. Int J Biol Macromol 2024;254:127691. https://doi.org/10.1016/j.ijbiomac.2023.127691.
[121] Zayed H, Saleh S, Omar A, Saleh A, Salama A, Tolba E. Development of collagen-chitosan dressing gel functionalized with propolis-zinc oxide nanoarchitectonics to accelerate wound healing. Int J Biol Macromol 2024;261:129665. https://doi.org/10.1016/j.ijbiomac.2024.129665.
[122] Zhou Z, Xun J, Wu C, Ji C, Ji S, Shu F, Wang Y, Chen H, Zheng Y, Xiao S. Acceleration of burn wound healing by micronized amniotic membrane seeded with umbilical cord-derived mesenchymal stem cells. Mater Today Bio 2023;20:100686. https://doi.org/10.1016/j.mtbio.2023.100686.
[123] Liu L, Yao S, Mao X, Fang Z, Yang C, Zhang Y. Thermosensitive hydrogel coupled with sodium ascorbyl phosphate promotes human umbilical cord-derived

mesenchymal stem cell-mediated skin wound healing in mice. Sci Rep 2023;13: 11909. https://doi.org/10.1038/s41598-023-38666-w.

[124] Davidson J, Yu F, Opalenik S. Splinting strategies to overcome confounding wound contraction in experimental animal models. Adv Wound Care (New Rochelle) 2013;2:142–8. https://doi.org/10.1089/wound.2012.0424.

[125] Tang JN, F.Halaseh F, Khan N, Zaki DP, Ziegler ME, Sayadi LR, Evans GRD, Widgerow A. 3D-printed wound chambers: a novel splint system wound healing research. Wounds Int 2021;12:54–8.

[126] Baek S, Jang U, Shin J, Kim J, Kim J, Lee J. Shape memory alloy as an internal splint in a rat model of excisional wound healing. Biomed Mater 2021;16:025002. https://doi.org/10.1088/1748-605X/abda89.